Synthesis and Characterization of Sulfonated Poly(ethylene terephthalate)/Montmorillonite Nanocomposites

Yang Li, Jinghong Ma, Yiming Wang, Borun Liang

State Key Laboratory for the Modification of Chemical Fibers and Polymer Materials, Donghua University, Shanghai 200051, People's Republic of China

Received 24 May 2004; accepted 5 January 2005
DOI 10.1002/app.22108
Published online in Wiley InterScience (www.interscience.wiley.com).

ABSTRACT: Sulfonated poly(ethylene terephthalate) (SPET)/montmorillonite nanocomposites were prepared by *in situ* intercalative polymerization. The microstructure, morphology, and properties of the nanocomposites were studied with wide-angle X-ray diffraction, transmission electron microscopy, atomic force microscopy, differential scanning calorimetry, and thermogravimetric analysis. The results indicated that an increase in the —SO_3Na content improved the dispersion of organically modified montmorillonite in the SPET ionomer matrix, and the dispersed layered silicates in the SPET matrix acted as nucleating agents in SPET crystallization processes and improved the thermal stability of SPET. © 2005 Wiley Periodicals, Inc. J Appl Polym Sci 98: 1150–1156, 2005

Key words: ionomers; nanocomposites; X-ray

INTRODUCTION

Layered-silicate-based polymer nanocomposites have attracted considerable technological and scientific interest in recent years. This technological interest has stemmed from the dramatic enhancements in the physical, thermal, and mechanical properties of polymer-based materials with a minimal increase in the density as a result of a low inorganic loading.[1–7]

Poly(ethylene terephthalate) (PET) is a low-cost, high-performance polymer that finds use in a wide variety of applications.[8–10] With only minor differences in the molecular weight and modifications, PET is used in textiles (clothes, curtains, and furniture upholstery), reinforcements of tires and rubber goods, and food and beverage packaging (water, soft drink and isotonic beverage bottles, sauce and jam jars, etc.). PET/montmorillonite (MMt) can be prepared by solution intercalation, *in situ* polymerization, and melt intercalation.[11–13] Dispersed MMt on the nanometer scale can improve the crystallizability, mechanical strength, gas-barrier properties, and thermal properties: the higher the degree of delamination in polymer/clay nanocomposites, the greater the enhancement of these properties.[14–20] Barber et al.[21] and Chisholm et al.[22] investigated PET and poly(butylene terepthalate) (PBT) ionomer/MMt composites made by melt extrusion and discovered that low levels of sulfonation in the polyester ionomers resulted in exfoliated clay nanocomposites. Ion-containing PET copolymers can be readily produced by the melt copolymerization of dimethyl terephthalate (DMT), dimethyl-5-sodiosulfoisophthalate (DMSIP), and ethylene glycol (EG). Because the level of sodium sulfonate (—SO_3Na) groups in the copolymers under investigation is 8 mol % or less, the copolymers fall into the category of ion-containing polymers, which are called *ionomers*. As a result, the sulfonated poly(ethylene terephthalate) (SPET) copolymers are called PET ionomers. The rheological and solid-state properties of SPET suggest that the —SO_3Na groups aggregate together to form small ionic domains.[23]

In this article, we report the synthesis of PET ionomer/MMt nanocomposites by *in situ* polymerization. The objective of this study is to evaluate the effects of the —SO_3Na content on the dispersion of MMt in the polymer matrix and MMt on the thermal and crystallization properties of the nanocomposites.

EXPERIMENTAL

Materials

Organophilically treated montmorillonite (OMMT), under the trade name DK0, was supplied by Zhejiang Fenghong Clay Co. (Zhejiang, China). MMt was treated with hexadecyl trimethyl ammonium chloride and had a cation-exchange capacity of 110 mequiv/100 g. DMT, DMSIP, and EG were purchased from Yizheng Chemical Fiber Co., Ltd. (Jiangsu, China). Triphenyl phosphite, zinc acetate, and antimony tri-

Correspondence to: B. Liang (bliang@dhu.edu.cn).

TABLE I
Compositions of the Polymer and the Composites

Sample	Molar ratio (DMSIP/DMT)	OMMT ratio (wt %)	Intrinsic viscosity (dL/g)
PET	0/100	0	0.548
SPET2	2/98	0	0.506
SPET4	4/96	0	0.506
SPET6	6/94	0	0.500
SPET8	8/92	0	0.580
SPET2M5	2/98	5	0.595
SPET4M5	4/96	5	0.526
SPET6M5	6/94	5	0.505
SPET8M5	8/92	5	0.528
PETM5	0/100	5	0.571

oxide were obtained from Shanghai Chemical Reagent Corp. (Shanghai, People's Republic of China).

Sample preparation

PET ionomers were prepared by the melt polymerization of DMT, DMSIP, and EG in a way similar to the polycondensation of PET. A representative polymerization procedure was as follows: 190.30 g (0.98 mol) of DMT, 5.92 g (0.02 mol) of DMSIP, 200 g (3.22 mol) of EG, 0.080 g of zinc acetate,0.056 g of antimony trioxide, and 0.032 g of triphenyl phosphite were charged to a 500-mL autoclave that was preheated to 100°C. The monomer mixture was then heated to 220°C at a rate of 1.0°C/min under atmospheric pressure, and these conditions were maintained until most of the methanol byproduct was removed by distillation. The mixture was then subjected to a gradual reduction in pressure while the temperature was simultaneously increased to 275°C at a rate of 1.0°C/min. After 120 min under a vacuum of 40–80 Pa, the melt was pelletized under cold water.

The ionic content of the ionomer is based on the molar percentage of DMSIP present in the copolymer. The previously detailed polymerization procedure was for the production of 2.0 mol % PET ionomer containing 2 mol of DMSIP to 98 mol of DMT; PET/MMt and SPET/MMT nanocomposites were prepared with the same polymerization procedure, and OMMT was added to the reactor with the monomers. The compositions of the polymer and the composites used in this study are given in Table I.

Characterization

Wide-angle X-ray diffraction (WAXD) patterns were recorded with a Rigaku Dmax 2550VB/PC diffractometer (Rigaku, Tokyo, Japan) equipped with Ni-filtered Cu Kα radiation (λ = 1.54 Å). The voltage and current of the X-ray tubes were 40 kV and 40 mA, respectively; corresponding data were collected from 2.0 to 10° at a scanning rate of 1.5°/min.

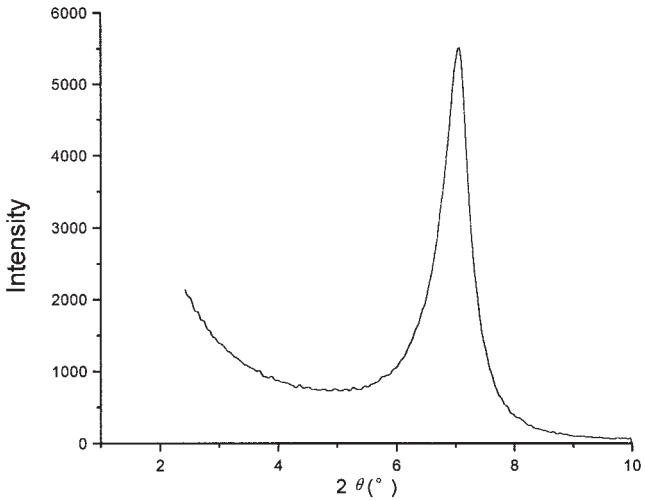

Figure 1 WAXD pattern of OMMT.

Transmission electron microscopy (TEM) micrographs were obtained on a JEM-1200EXII transmission electron microscope (JEOL, Tokyo, Japan) with an acceleration voltage of 120 kV. Ultrathin sections about 100 nm thick were cut with an LKB-5 microtome (LKB Co., Ltd., Uppsala, Sweden) equipped with a diamond knife and placed in a 200-mesh copper grid.

Atomic force microscopy (AFM) measurements were carried out with a Digital Instrument (USA Veeco Instruments, Inc., Woodbury, NY) Nanoscope IV. Before the AFM observations, the materials were melt-pressed into 1-mm films; the film surface had to be checked by optical microcopy to ensure a continuous and flat surface without breakage or damage. The tapping mode was used.

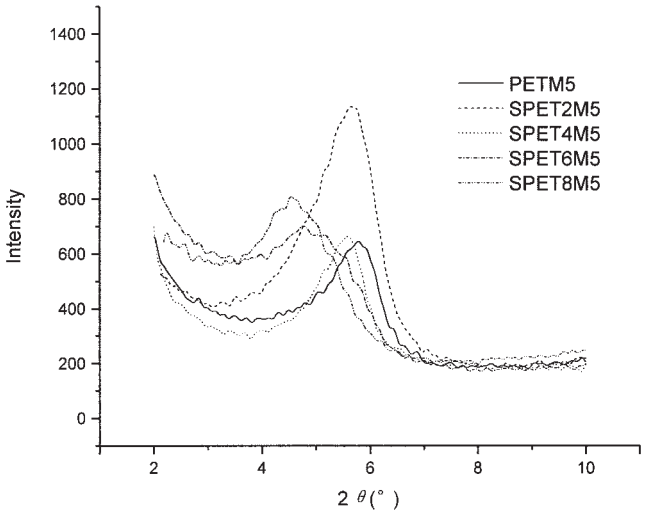

Figure 2 WAXD patterns of PETM5, SPET2M5, SPET4M5, SPET6M5, and SPET8M5.

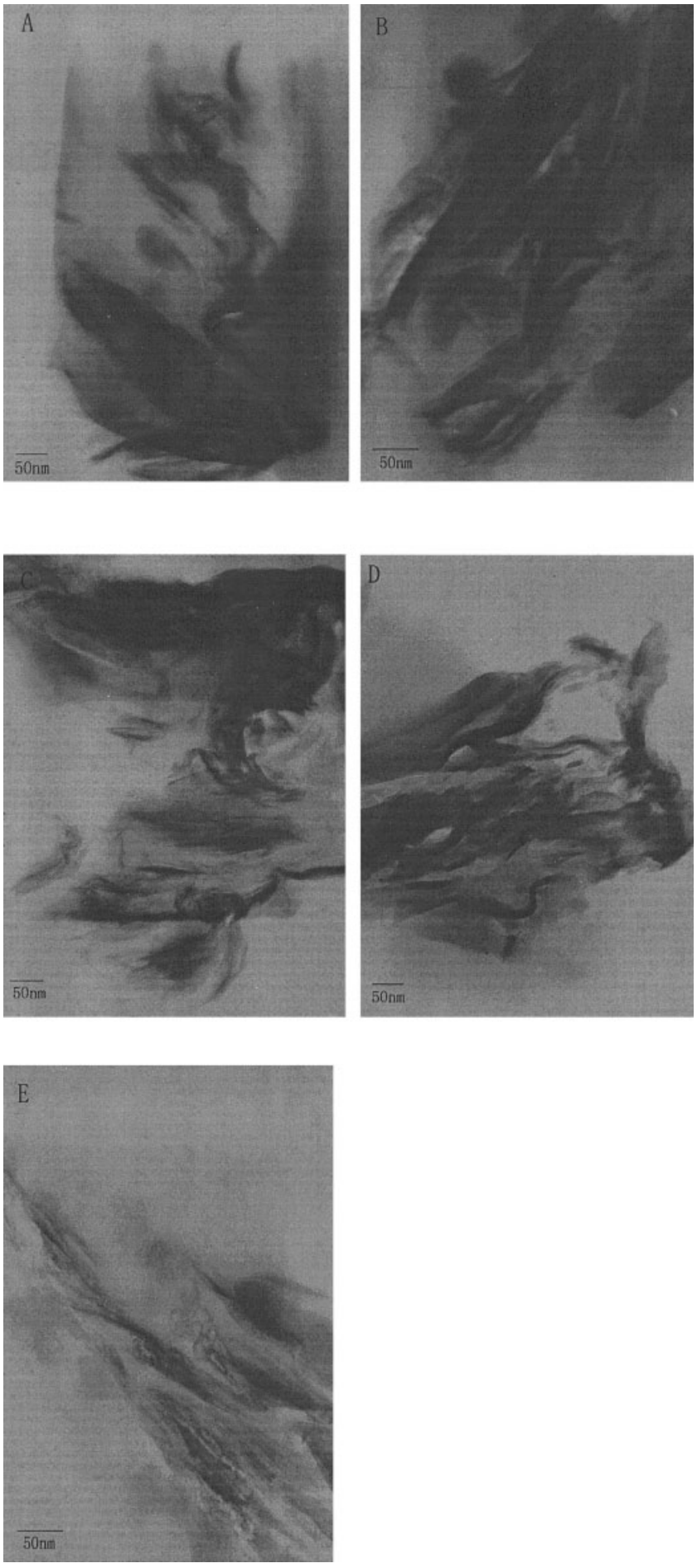

Figure 3 TEM images of the nanocomposites with 5 wt % OMMT: (A) PETM5, (B) SPET2M5, (C) SPET4M5, (D) SPET4M5, and (E) SPET8M5.

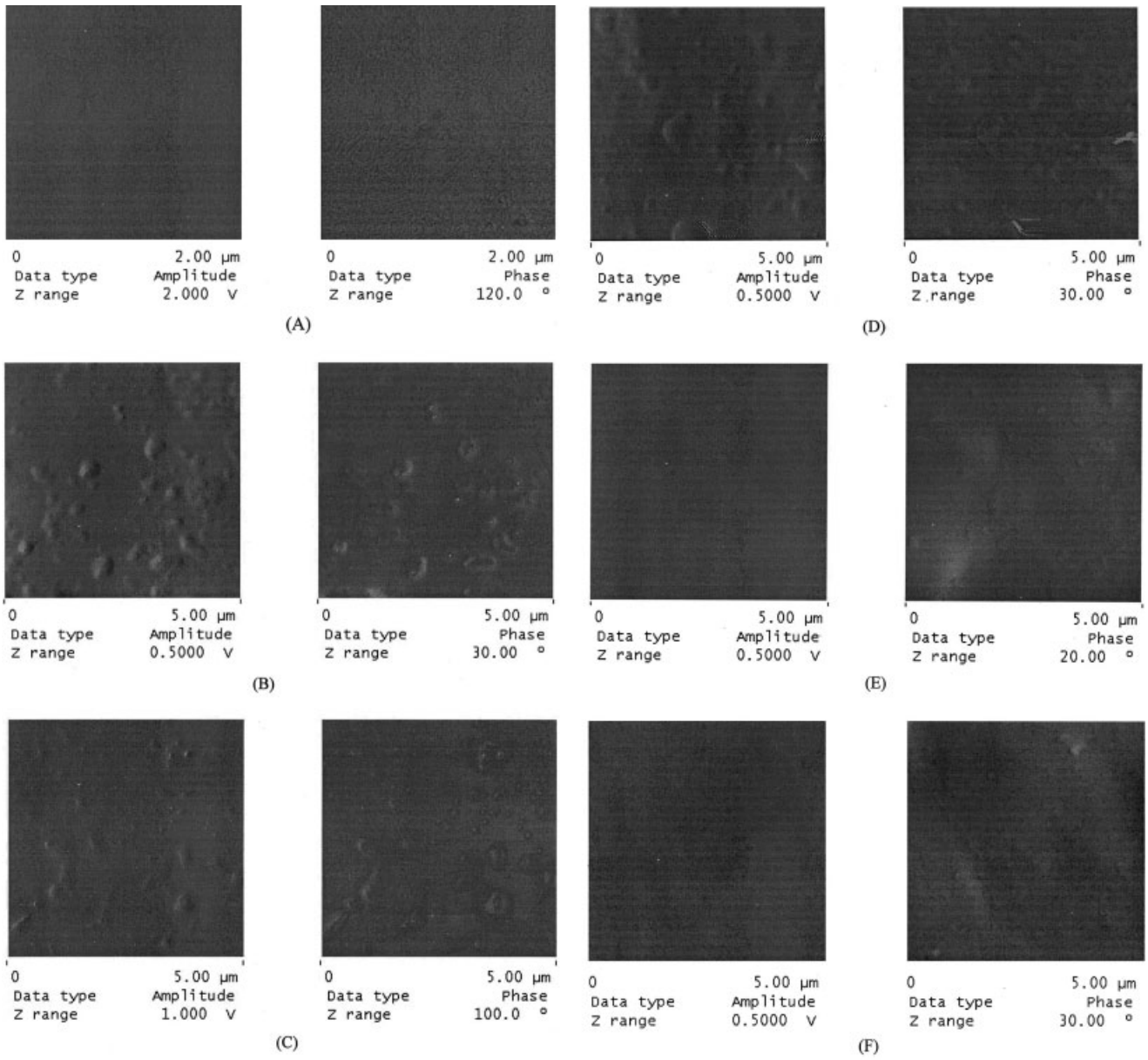

Figure 4 AFM micrographs of (A) PET, (B) PETM5, (C) SPET2M5, (D) SPET4M5, (E) SPET6M5, and (F) SPET8M5. The micrographs on the left are amplitude images, and those on the right are phase images.

Differential scanning calorimetry (DSC) was performed on a PerkinElmer DSC-7 differential scanning calorimeter (PerkinElmer, Wellesley, MA) at a heating or cooling rate of 10°C/min and a nitrogen flow rate of 100 mL/min.

Thermogravimetric analysis (TGA) experiments were conducted on a PerkinElmer TGA-7 thermogravimeter at a heating rate of 20°C/min under a nitrogen flow rate of 40 mL/min.

RESULTS AND DISCUSSION

Dispersibility of MMt in SPET

The WAXD curves of OMMT are presented in Figure 1; the diffraction peak appears at $2\theta = 7.08°$, corresponding to a *d*-spacing of 12.47 Å. The WAXD patterns of PETM5, SPET2M5, SPET4M5, SPET6M5, and SPET8M5 containing 5 wt % OMMT are shown in Figure 2; the diffraction peaks of PETM5, SPET2M5, SPET4M5, SPET6M5, and SPET8M5 appear at 2θ values of 5.82, 5.68, 5.58, 4.81, and 4.61°, respectively. The interlayer spacing increases from 12.47 Å for the base distance of OMMT to 15.16, 15.53, 15.81, 18.33, and 19.12 Å for PETM5, SPET2M5, SPET4M5, SPET6M5, and SPET8M5,respectively; this indicates the insertion of PET and SPET. The gallery expansion of MMt in the SPET matrix increases by 0.37–3.96 Å with increasing DMSIP content from 2 to 8 mol %. The shift from 15.53 to 19.12 Å in the *d*-spacing of layered silicates in SPET/MMt nanocomposites can be ascribed to the

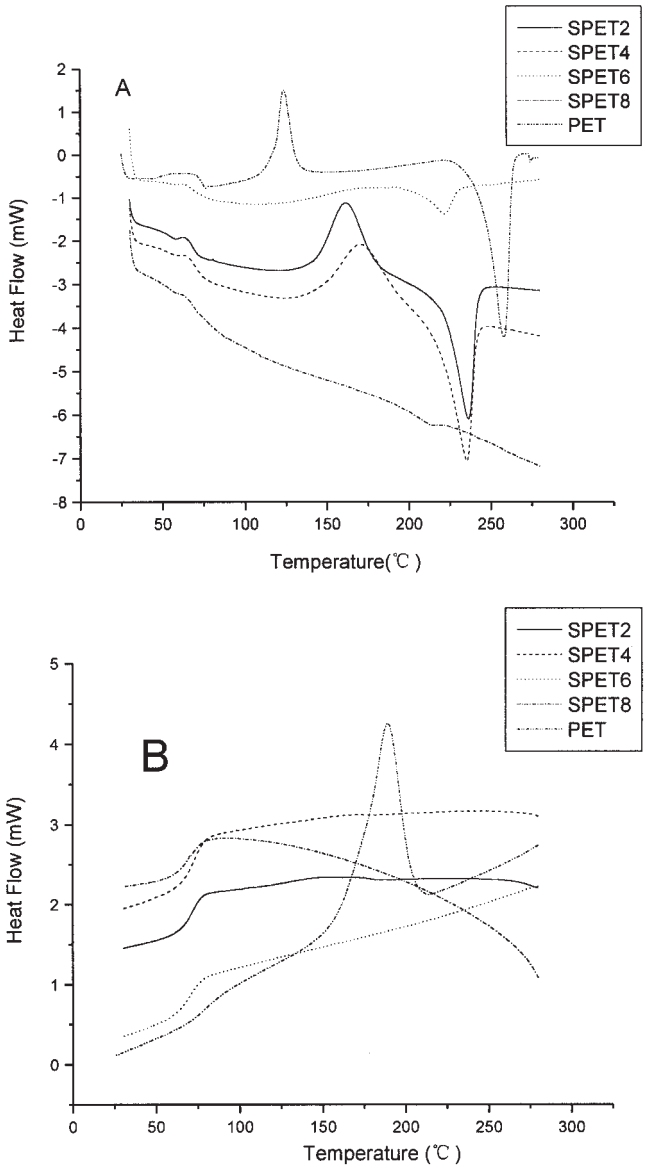

Figure 5 DSC (A) heating curves and (B) cooling curves for PET and SPET ionomers.

fact that at a low concentration of sodium sulfonate, ion pairs along the ionomer chains may also interact with the platelet surfaces by dipole–dipole interactions; as the concentration of —SO_3Na groups is increased, the stronger interaction leads to a bigger gallery spacing of MMt in PET ionomers. Further evidence of the organo-MMt dispersion in SPET has been cross-checked by TEM and AFM observations.

Morphology

TEM micrographs are presented in Figure 3(A–E). The dark lines are the intersections of sheet layers. Figure 3(A,B) shows the TEM photographs of PETM5 and SPET2M5, respectively. The silicate layers are intercalated by the polymer matrix, and some of them are agglomerated with a size level about 15–20 nm. For the nanocomposites containing 4–8 mol % —SO_3Na groups, Figure 3(C–E) shows that some clay is exfoliated in the polymer matrix. The existence of the peaks in the XRD patterns of these samples should be attributed to these unexfoliated layers (see Fig. 2); the spaces between the silicate layers in SPET/MMt becomes larger with an increasing ion content.

Figure 4(B–F) shows the AFM amplitude images and phase images of the polymer/MMt nanocomposites. The silicate particles dispersed in the matrix become smaller with increasing DMSIP content; the average tactoid dimension ranges from 500 nm to 100 nm. Figure 4(B–D) shows that in the matrix with a low content of DMSIP, the silicate platelets are agglomerated. In SPET6M5 and SPET8M5, the silicate particles are finely dispersed in the nanocomposites with an

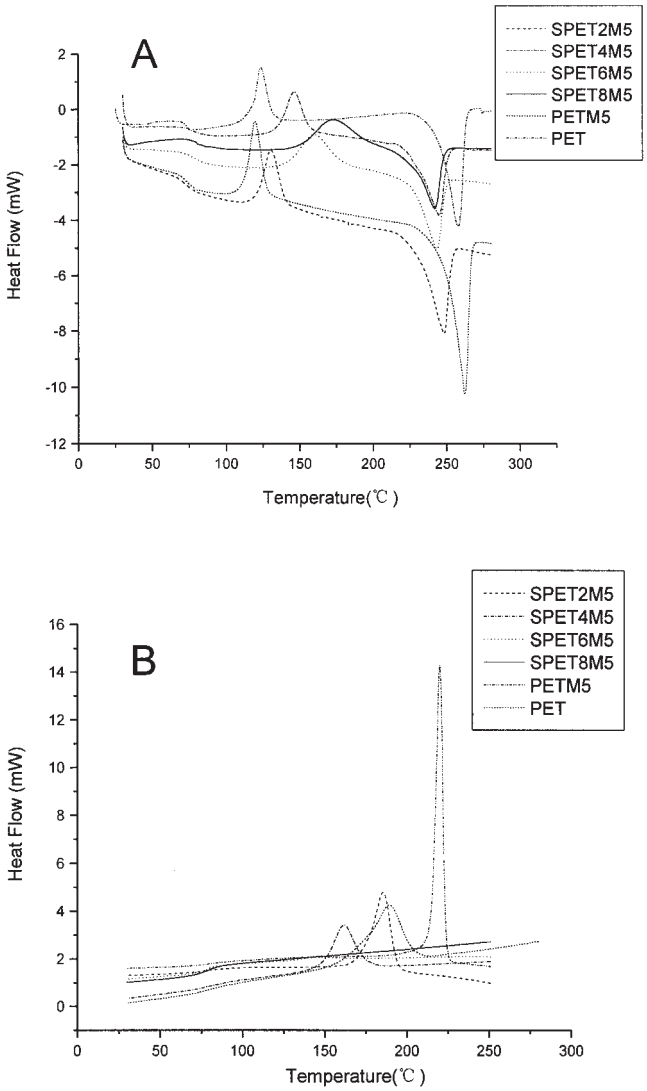

Figure 6 DSC (A) heating curves and (B) cooling curves for PET, PET/MMt, and SPET/MMt.

average size of 100 nm. No intersections of sheet layers are detected; the AFM image only shows the silicate platelets dispersed because the method to make samples for AFM is different from that for TEM.

Thermal and crystallization properties

Figure 5(A,B) illustrates the thermal behavior of pure PET and SPET ionomers at different temperatures. The existence of ionic groups lowers the crystallizability, the cold-crystallization peak shifts to the high-temperature region, and the melting peak shifts to the low-temperature region with the —SO_3Na group content increasing. In comparison with pure PET, the crystallization peaks from the melt were not detected for the SPET ionomers. When the ionomer contains 8 mol % DMSIP, the polymer has nearly no crystallizability, even in cold crystallization; this is because the existence of the —SO_3Na group lowers the regularity of the PET molecular chain. The ionic clusters in the ionomer matrix constrain the movement of the polymer chain; thus, the crystal growth is to some extent affected.

Figure 6 shows a comparison of a series of DSC thermograms of nanocomposites with a clay concentration of 5 wt %. The results indicate that the dispersed MMt sheets greatly promote the crystallization of ionomers. For SPET2M5 and SPET4M5, the temperatures of cold crystallization are shifted to a lower temperature region. The crystallization behavior of SPET2M5 is similar to that of PET. For SPET6M5, there are two strong peaks of crystallization from the glassy state and from the melt state. Even for SPET8M5, with the addition of MMt, a cold-crystallization peak appears; it can be thought that the improvement of the ionomer crystallizability is due to the nucleus effect of the nanoparticles of clay or due to the nanoparticles combining with the polymer matrix, which forms a nucleus nanostructure in the nanocomposite systems. The silicate dispersed at the nanometer level weakens the interactions of ion pairs of ionomers.

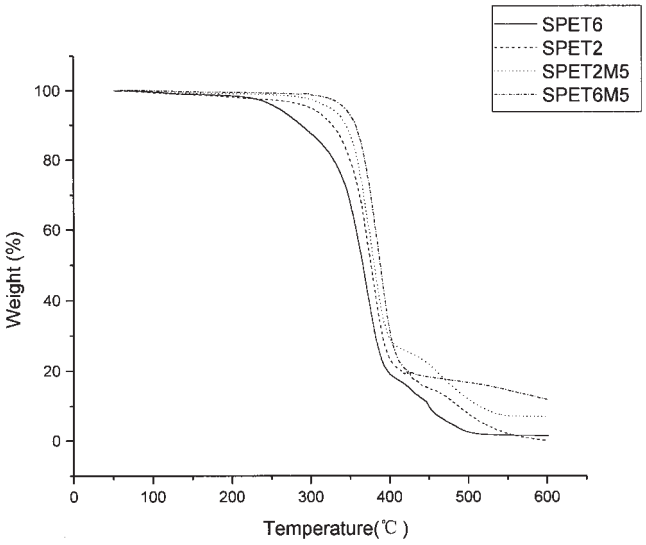

Figure 7 TGA curves of SPET2, SPET6, SPET2M5, and SPET6M5.

TABLE II
Heat Resistance of SPET and SPET/MMt Nanocomposites

Sample	Temperature for 5% weight loss (°C)	Temperature for 10% weight loss (°C)	Weight retention at 600°C (%)
SPET2	299	327	0.0
SPET6	258	288	1.4
SPET2M5	324	344	6.9
SPET6M5	343	357	11.8

Figure 7 presents the TGA results of ionomers and ionomer/MMt nanocomposites. The SPET/MMt nanocomposites show delayed decomposition temperatures in comparison with SPET. The temperatures for 5% weight loss and 10% weight loss and the weight retention at 600°C in TGA diagrams are summarized in Table II.

The effect of MMt on the temperatures for 5% weight loss and 10% weight loss is evident; when 5 wt % MMt was introduced to SPET, the decomposition temperatures increased by 25 and 17°C for SPET2M5 and by 85 and 69°C for SPET6M5, respectively. It is thought that the strong interaction between MMt and ionomers improved the thermal resistance properties of the intercalated nanocomposites. MMt possesses high thermal stability, and its layer structure exhibits a great barrier effect to stop the evaporation of the small molecules generated in the thermal decomposition process and effectively limits the continuous decomposition of SPET.

CONCLUSIONS

SPET/MMt nanocomposites were successfully prepared by intercalation polymerization. With an increasing content of DMSIP in SPET, a better dispersion of the MMt layers in the SPET matrix was verified by WAXD, TEM, and AFM. Through comparative DSC studies, the loading of silicates showed a heterogeneous nucleation effect on the crystallization of SPET. Because of the dispersion of MMt layers and strong interactions between the SPET matrix and the MMt layers, the nanocomposites showed better thermal stability than virgin SPET.

References

1. Ki, H. W.; Min, H. C.; Chong, M. K.; Mingzhe, X.; In, J. C.; Min, C. J. Sun, W. C.; Hyun, H. S. J Polym Sci Part B: 2002, 40, 1454.

2. Pralay, M.; Pham, H. N.; Masami, O. Macromolecules 2002, 35, 2042.
3. Fornes, T. D.; Yoon, P. J.; Hunter, D. L.; Keskkula, H.; Paul, D. R. Polymer 2002, 87, 5915.
4. Yao, K. J.; Song, M.; Hourston, D. J.; Luo, D. Z. Polymer 2002, 43, 1017.
5. Tae, H. K.; Sung, T. L.; Chung, H. L.; Hyoung, J. C.; Myung, S. J. J Appl Polym Sci 2003, 87, 2106.
6. Qiwen, D.; Deyue, Y. Polym Prepr 2003, 44, 1140.
7. In-Joo, C.; Thomas, T. A.; Ho-Cheol, K. Polym Prepr 2000, 41, 591.
8. Hwang, S. H.; Paeng, S. W.; Kim, J. Y.; Huh, W. Polym Bull 2003, 49, 329.
9. Wang, D.; Zhu, J.; Yao, Q.; Wilkie, C. A. Chem Mater 2002, 14, 3837.
10. Lebaron, P. C.; Wang, Z.; Pinnavaia, T. J Appl Clay Sci 1999, 12, 11.
11. Ou, C. F.; Ho, M. T.; Lin, J. R. J Polym Res 2003, 10, 127.
12. Yang, C. K.; Zhi, B. Y.; Chuan, F. Z. J Appl Polym Sci 2002, 85, 2677.
13. Davis, C. H.; Mathias, L. J.; Gilman, J. W.; Schiraldi, D. A.; Shields, J. R.; Trulove, P.; Sutto, T. E.; Delong, H. C. J Polym Sci Part B: Polym Phys 2002, 40, 2661.
14. Chang, J. H.; Kim, S. J.; Joo, Y. L.; Im, S. Polymer 2004, 45, 919.
15. Imai, Y.; Inukai, Y.; Tateyama, H. Polym J 2003, 35, 230.
16. Ke, Y.; Long, C.; Qi, Z. J Appl Polym Sci 1999, 71, 1139.
17. Zhang, G.; Shichi, T.; Takagi, K. Mater Lett 2003, 51, 1858.
18. Sanchez-Solis, A.; Garcia-Rejont, A.; Manero, O. Macromol Symp 2003, 192, 281.
19. Wang, Y.; Shen, C.; Li, H.; Li, Q.; Chen, J. J Appl Polym Sci 2004, 91, 308.
20. Liu, W.; Tian, X.; Cui, P.; Li Y.; Zheng, K.; Yang, Y. J Appl Polym Sci 2004, 91, 1229.
21. Barber, G. D.; Bellman, S. P.; Moore, R. B. Annual Technical Conference Proceedings, Nashville, TN, May, 2003.
22. Chisholm, B. J.; Moore, R. B.; Burber, G. Macromolecules 2002, 35, 5508.
23. Gorda, K. R.; Peiffer, D. G. J Polym Sci Part B: Polym Phys 1992, 30, 281.